IOP Publishing Journal of Physics B: Atomic, Molecular and Optical Physics
J. Phys. B: At. Mol. Opt. Phys. **53** (2020) 035502 (9pp) https://doi.org/10.1088/1361-6455/ab56db

Lock-in-detection in ^{87}Rb–^{129}Xe/^{131}Xe atom spin gyroscopes

Sangkyung Lee, Sin Hyuk Yim, Tae Hyun Kim, Zaeill Kim and Kyumin Shim

Agency for Defense Development, Daejeon 34186, Republic of Korea

E-mail: sklee82@add.re.kr

Received 28 March 2019, revised 2 September 2019
Accepted for publication 12 November 2019
Published 17 January 2020

Abstract

We demonstrate a ^{87}Rb–^{129}Xe/^{131}Xe atom spin gyroscope, where two stage lock-in-amplifiers are applied to measure the shift of the NMR frequency. The NMR frequency shifts and their Allan deviation are analyzed during on- and off-resonance operation. The filter effects of the lock-in-amplifiers are investigated in terms of the Allan deviation. Based on the dual species operation, we achieve an angular random walk of 1.11 deg $h^{-1/2}$ for the rotation rate. The slightly off-resonance operation reveals that the NMR insensitive white noise of the ^{131}Xe signal limits the angular random walk of our system.

Keywords: atom spin gyroscope, NMR gyroscope, lock-in-detection

(Some figures may appear in colour only in the online journal)

1. Introduction

Spin-polarized noble gas atoms are widely used in MRI [1–3], magnetometers [4], rotation sensing [5–8], and even studies of fundamental symmetries [9, 10]. They have paved the way to precise measurements of a magnetic field and rotation, based upon their long spin coherence time. Nowadays, atom spin gyroscopes have attracted attention as potentially high precision, low power, and compact gyroscopes [7, 11]. Recently, comagnetometer-based gyroscopes were reported [6, 12]. The comagnetometer type requires the spin exchange relaxation free condition, where a bias B-field is quite low, below 10 nT and the temperature is over 150 °C, to increase the spin-exchange rate [13]. Such gyroscopes would allow the lowest angular random walk, below 0.002 deg $h^{-1/2}$ by self-cancellation of the magnetic field transient as well as magnetic field gradient [6]. The required conditions, however, are somewhat strict. More practically, Northrop Grumman have developed a dual species atom spin gyroscope with a 10cc physical package, whose angular random walk is 0.005 deg $h^{-1/2}$ [14]. In contrast to the comagnetometer type, the effect of the magnetic field noise on the NMR frequency shift can be subtracted by measuring the NMR frequency shifts of two isotopes simultaneously. We also have developed an atom spin gyroscope based on the dual species approach.

Atom spin gyroscopes, referred to as NMR gyroscopes, measure the shift in the NMR frequency of noble gas atoms by converting nuclear spin precession to the corresponding voltage through lock-in-amplifiers [15]. When the transverse AC magnetic field is resonant on the NMR frequency, the nuclear magnetic moment starts to precess at the NMR frequency, proportional to the bias magnetic field in a non-rotating frame. In a rotating frame, the obtained signal is very sensitive to the rotation rate as well as the magnetic field. On the other hand, in the off-resonance operation, it is insensitive to the magnetic field so that the magnetic field noise-free angular random walk limit of the system can be achieved. But the filter effects of lock-in-amplifiers should be considered carefully.

In this paper, we analyze the measured NMR frequency shifts obtained by two stage lock-in-amplifiers, theoretically and experimentally. The Allan deviation of the rotation rate is investigated by considering the filter effects of lock-in-amplifiers, in the dual species mode to reduce the magnetic field noise effect, and in the off-resonance mode to reveal the magnetic field noise-free angular random walk limit.

2. Theory

In alkali-noble gas atomic spin gyroscopes, alkali atoms are utilized to sense the nuclear magnetic field of the noble gas

atoms, as well as to polarize the noble gas atom spins, assisted by spin-exchange collisions [16]. To diminish the effect of any unwanted noise and to selectively sense the transverse magnetic field B_x or B_y, the bias B_z field is modulated at the Rb Larmor frequency. This technique is called parametric modulation [17, 18]. The magnetic moment of rubidium can be expanded by the sum of harmonics whose frequencies are integer multiples of the modulation angular frequency $\omega_{\rm mod}$

$$\begin{aligned} M^+ &= M_x^{\rm Rb} + iM_y^{\rm Rb} \\ &= i\tau\gamma_{\rm Rb}M_z^{\rm Rb}(B_x + iB_y)\sum_{n=-\infty}^{n=\infty}\frac{J_n^2(\xi)}{1 + i(\omega_z^{\rm Rb} + n\omega_{\rm mod})\tau} \\ &+ J_n(\xi)\sum_{p=1}^{\infty}\frac{J_{n-p}(\xi) + J_{n+p}(\xi)}{1 + i(\omega_z^{\rm Rb} + n\omega_{\rm mod})\tau}\cos p\omega_{\rm mod}t \\ &+ i\frac{J_{n-p}(\xi) - J_{n+p}(\xi)}{1 + i(\omega_z^{\rm Rb} + n\omega_{\rm mod})\tau}\sin p\omega_{\rm mod}t, \end{aligned} \tag{1}$$

where $M_x^{\rm Rb}$, $M_y^{\rm Rb}$, and $M_z^{\rm Rb}$ are the Rb magnetic moments along the x, y, and z directions, respectively. τ is the lifetime of Rb spin, $\gamma_{\rm Rb}$ is the gyromagnetic ratio of Rb atoms, and ξ is the ratio of the bias magnetic field modulation amplitude to the modulation frequency, given by $\xi = \omega_{\rm amp}/\omega_{\rm mod}$. $\omega_z^{\rm Rb}$ is the Larmor frequency of Rb and $\omega_{\rm amp}$ is the amplitude of the bias magnetic field modulation in angular frequency domain, given by $\omega_{\rm amp} = \gamma_{\rm Rb}\,B_{\rm mod}$ where $B_{\rm mod}$ is the amplitude of the bias magnetic field modulation. $J_n(\xi)$ represents the Bessel function. The transverse $B_x + iB_y$ field can be represented by the sum of the external B_x field, the noble gas induced B-field, and the residual DC B-field:

$$B_x + iB_y = B_{xd}\cos\omega_{xd}t + \psi B_{\rm xe}e^{-i(\omega_{xd}t+\phi_{\rm xe}-\frac{\pi}{2})} + B_{\rm res}^+, \tag{2}$$

where ω_{xd} is the angular frequency of the transverse AC B_x field, B_{xd} is the amplitude of the transverse AC B_x field, and $B_{\rm res}^+$ is the residual transverse DC magnetic field, given as $B_{\rm res}^+ = B_{{\rm res},x} + iB_{{\rm res},y}$ where $B_{{\rm res},x}$ and $B_{{\rm res},y}$ are the residual DC magnetic field along the x and the y directions, respectively. $B_{\rm xe}$ is the nuclear magnetic field from the noble gas atom, given as $B_{\rm xe} = \frac{2}{3}\kappa_0\mu_0K_0$. κ_0 is the enhancement factor due to Fermi contact [19], μ_0 is the vacuum permeability, and K_0 is the mean angular momentum of the noble gas atom nuclear spin. In a steady state, the tip angle ψ is given by

$$\psi = \frac{\gamma_{\rm xe}B_{xd}T_2\sqrt{1 + (T_2\Delta\omega)^2}}{1 + (T_2\Delta\omega)^2 + (\gamma_{\rm xe}B_{xd})^2T_1T_2}, \tag{3}$$

where $\gamma_{\rm xe}$ is the gyromagnetic ratio of the noble gas atom. The gyromagnetic ratios of the ^{129}Xe atoms and of the ^{131}Xe atoms are given as $\gamma_{129} = -2\pi \times 11.86\,{\rm Hz}/\mu{\rm T}$ and $\gamma_{131} = 2\pi \times 3.52\,{\rm Hz}/\mu{\rm T}$, respectively. $\Delta\omega$ is the detuning of the B_x field with respect to the Larmor frequency of the noble gas atom, i.e. $\Delta\omega = \omega_{xd} - |\gamma_{\rm xe}B_0 + \Omega|$ where Ω is the rotation rate and B_0 is the magnitude of the bias DC B-field. The phase delay of the nuclear precession $\phi_{\rm xe}$ is determined by $\tan\phi_{\rm xe} = \Delta\omega T_2$. T_1 and T_2 are the longitudinal and transverse lifetime of the nuclear precession. Here, we assume that the response of the noble gas atom follows adiabatically the bias magnetic field change and the rotation rate change, i.e. $\frac{1}{|B_0|}\frac{d|B_0|}{dt} \ll |\gamma_{\rm xe}B_0|$ and $\frac{1}{|\Omega|}\frac{d|\Omega|}{dt} \ll |\gamma_{\rm xe}B_0|$. Hence the signal is linearly proportional to the magnetic field change and the rotation rate change.

In order to measure the NMR frequency shift, two stage lock-in-amplifiers can be used. The first lock-in-amplifier uses the demodulation reference signal, $V_{1L}\cos(\omega_{\rm mod}t + \phi_{\rm mod})$ where V_{1L} is the amplitude of the reference signal, $\omega_{\rm mod}$ is the angular frequency of the parametric modulation, and $\phi_{\rm mod}$ is its phase delay. The first lock-in-amplifier, in conjunction with a parametric modulation with $\phi_{\rm mod} \approx 0$, enables it to only sense the B_y field on which precession of the noble gas atoms is imprinted. With a help of Fourier and inverse Fourier transforms, the lock-in-signal passing through the first lock-in-amplifier, can be written as

$$\begin{aligned} y_{1L}^+(t) &= \frac{1}{2\pi}\int_{-\infty}^{\infty}d\nu H_{1L}(\nu)e^{i\nu t} \\ &\times \int_{-\infty}^{\infty}dt'M^+(t')V_{1L}\cos(\omega_{\rm mod}t' + \phi_{\rm mod})e^{-i\nu t'}, \end{aligned} \tag{4}$$

where $H_{1L}(\nu)$ is the transfer function of the band pass filter in the first lock-in-amplifier. The bandpass filter passes signals with the NMR frequency of the selected Xe isotope. Strictly, the integral over t' from $-\infty$ to ∞ describes non-casual cases because $t < t'$ contribution is included. We consider the system in the steady state after a long time, i.e. $t \to \infty$. Equation (4) where the integral over t' extends to infinity is, therefore, able to describe casual cases, approximately. The second stage lock-in-amplifier converts the sinusoidal signal originating from the precession of the noble gas atoms into a measurable voltage. For this, the transverse AC magnetic field to drive precession of the noble gas atoms is used as the demodulation reference, $V_{2L}\cos(\omega_{xd}t + \phi_{xd})$ where V_{2L} is the amplitude of the reference signal for the second stage lock-in-amplifier, ω_{xd} is the drive frequency, and ϕ_{xd} is the phase delay. In the same manner as the first lock-in-amplifier, a signal from the second lock-in-amplifier can be written as

$$\begin{aligned} y_{2L}^+(t) &= \frac{1}{2\pi}\int_{-\infty}^{\infty}d\nu H_{2L}(\nu)e^{i\nu t} \\ &\times \int_{-\infty}^{\infty}dt'y_{1L}^+(t')V_{2L}\cos(\omega_{xd}t' + \phi_{xd})e^{-i\nu t'}, \end{aligned} \tag{5}$$

where $H_{2L}(\nu)$ is the transfer function of the low pass filter in the second lock-in-amplifier. The low pass filter extracts a DC signal which contains the amplitude and phase information of the NMR precession. Similar to equation (4), equation (5) can describe approximately casual cases in the steady state. The used symbols and their meaning are summarized in tables A1 and A2 in appendix.

3. Experimental setup

The experimental setup for measuring the NMR frequency shifts is shown in figure 1(a). The Pyrex cubic cell is filled with ^{87}Rb vapor, 50 Torr of natural Xe, 250 Torr of N_2, and 5 Torr of H_2. Its dimension is $15 \times 15 \times 15\ {\rm mm}^3$. We chose the partial pressures with reference to [10]. The order of 100 Torr of the N_2 gas suppresses radiative decay of Rb by quenching

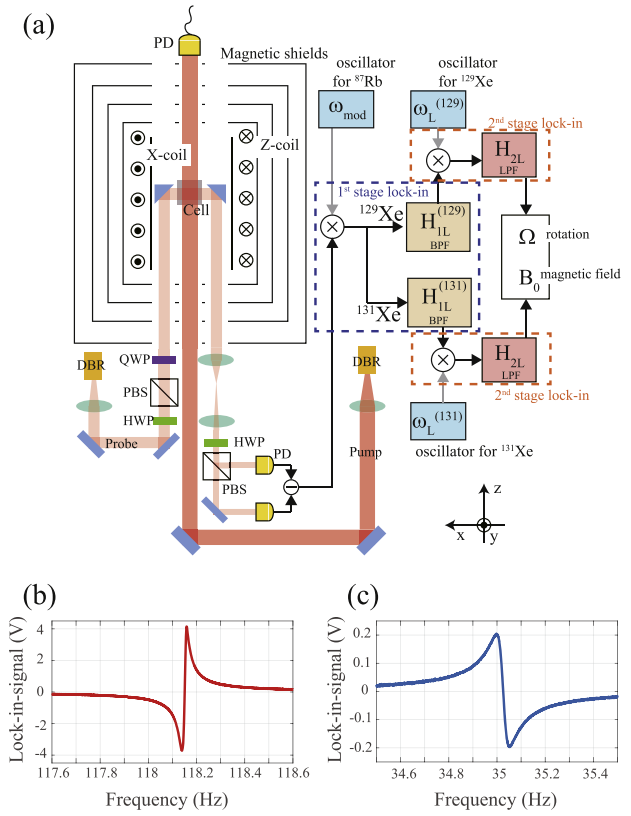

Figure 1. (a) Schematic diagram of the experimental setup. DBR: distributed Bragg reflector laser, PBS: polarization beam splitter, HWP: half wave plate, QWP: quarter wave plate, PD: photodiode, BPF: band pass filter for the precession signal of the selected Xe isotope, LPF: low pass filter. $H_{1L}^{(129)}$ and $H_{1L}^{(129)}$ denote the band pass filters in the first lock-in-amplifiers for ^{129}Xe and for ^{131}Xe, respectively. H_{2L} indicates the low pass filter in the second lock-in-amplifier. The black arrows indicate the signal flow. The gray arrows depict the reference signals. (b) Measured dispersion curves of ^{129}Xe. (c) Measured dispersion curves of ^{131}Xe.

the excited state of Rb [1]. The H_2 gas makes RbH coatings on the inner surface of the cell to increase the transverse relaxation time T_2 of ^{131}Xe [20]. The atomic cell is supported by a non-magnetic cell mount made from Polyether ether ketone (PEEK). The 2-layer AC heater, where currents flowing in opposite directions in the same wire pattern on both layers cancel the unwanted magnetic field generation, is mounted on the cell mount [21]. The temperature of the atomic cell reaches around 100 °C for frequent Rb–Xe spin-exchange collisions. 4 layer cylindrical magnetic shields (MS-1, Twinleaf) are used to reduce penetration of the unwanted external B-field. The built-in x, y, z bias coil and the gradient coil are installed on the inner surface of the innermost magnetic shield. The free induction decays were measured to verify characteristics of the atomic cell such as T_2 and B_{xe}. For the ^{129}Xe atoms (or ^{131}Xe), we obtained $T_2^{(129)} = 20s$ (or $T_2^{(131)} = 9$ s), and $B_{xe}^{(129)} = 100$ nT (or $B_{xe}^{(131)} = 9$ nT). The upper limit of the T_2 time is determined by the longitudinal relaxation time T_1. The inversion recovery method was used to measure the T_1 times [22]: $T_1^{(129)} = 27$ s for the ^{129}Xe atoms and $T_1^{(131)} = 12$ s for the ^{131}Xe atoms, respectively.

In order to apply the parametric modulation, a bias magnetic field is modulated at the Rb Larmor frequency, given as $B_z = B_0 + B_{\rm mod}\cos\omega_{\rm mod}t$ where B_0 is the DC bias magnetic field, 9.95 μT, $\omega_{\rm mod} = 2\pi \times 69.63$ kHz, and $B_{\rm mod}$ is the AC bias magnetic field amplitude, 10 μT. For the spin-exchange optical pumping, the ^{87}Rb atoms are optically pumped by a 120 mW DBL laser (PH795DBR120TS-L, Photodigm) whose frequency is tuned to the Rb D_1 line. The circular polarization of the pump laser populates Rb atoms into the selected Zeeman sublevel, $m_s = 1/2$ of the $^2S_{1/2}$ state, so that the Rb atoms are spin-polarized. The pressure broadening makes the hyperfine structure of Rb unresolved [1]. For atom spin gyroscope operation, a continuous weak B_x is applied, $B_{xd}(t) = B_{xd}^{(129)}\cos\omega_{xd}^{(129)}t + B_{xd}^{(131)}\cos\omega_{xd}^{(131)}t$ where $B_{xd}^{(129)} = 0.5$ nT, $B_{xd}^{(131)} = 10$ nT, $\omega_{xd}^{(129)} = 2\pi \times 118.15$ Hz, and $\omega_{xd}^{(131)} = 2\pi \times 35.022\,5$ Hz. The two frequency components drive the ^{129}Xe and ^{131}Xe Larmor precession, respectively.

Optical Faraday detection is utilized to detect the precession of the Xe atoms. In our setup, the probe laser (PH795DBR120TS-L, Photodigm) propagates along the x-direction so that the Faraday rotation angle depends on $M_x^{\rm Rb}$, the magnetic moment of the rubidium atoms along the x-direction on which the Xe atom precession is imprinted. The Faraday rotation is measured by a combination of a halfwave plate, a polarization beam splitter, and a balanced photo-detector. It is converted into a voltage signal by using the two stage lock-in-amplifiers, which are implemented by Labview FPGA (USB-7855R, NI). The sampling rate of the FPGA are 200 kHz, referred to its own clock. Because the Larmor frequencies of ^{129}Xe, ^{131}Xe, and ^{87}Rb are smaller than half the sampling rate of the FPGA, the FPGA lock-in-amplifiers are able to process the time-continuous Larmor precession signal in our system.

Each lock-in-amplifier consists of a mixer and a bandpass or low pass filter. The mixer is simply implemented by multiplying the two digitized values of the reference and the signal. The references for the lock-in-amplifiers are generated by the function generators (DG1022, Rigol for Rb, 33250A, Agilent for ^{129}Xe, and AFG3101C, Tektronix for ^{131}Xe) and they are synchronized by a 10 MHz clock signal from a low noise reference oscillator. The references are also used to modulate the bias B-field and the transverse B_x field. The main part of the FPGA lock-in-amplifiers is the numerical RC filter modeling. The FPGA calculates the recursion relation of a simple analog RC filter: $y_{out}(t_n) = (1\text{–}2\pi\ \Delta t f_c)\ y_{out}(t_{n-1}) + 2\pi\ \Delta t f_c\ y_{in}(t_{n-1})$ for a RC low pass filter and $y_{out}(t_n) = (1\text{–}2\pi\ \Delta t f_c)\ y_{out}(t_{n-1}) + (y_{in}(t_n) - y_{in}(t_{n-1}))$ for a RC high pass filter, where y_{in} and y_{out} are the input signal and the output signal. f_c is the cut-off frequency of the RC filter. Δt is the consumed time of a 1 cycle of the FPGA lock-in-amplifier, given by 5 μs in our experimental setup. n denotes the sample number.

In the first stage lock-in-amplifier for the ^{129}Xe signal, the 3 low pass filters with a cut-off frequency of 125 Hz and the 3 high pass filters with a cut-off frequency of 100 Hz are applied to extract the sinusoidal precession signal of ^{129}Xe:

$\nu_{1L,low}^{(129)} = 125$ Hz and $\nu_{1L,high}^{(129)} = 100$ Hz. The transfer function of the filters is given by $H_{1L}^{(129)}(\nu) = [1/(1 + i\nu/\nu_{1L,low}^{(129)})]^3$ $[(i\nu/\nu_{1L,high}^{(129)})/(1 + i\nu/\nu_{1L,high}^{(129)})]^3$. On the other hand, in the first stage lock-in-amplifier for the ^{131}Xe signal, the 8 low pass filters with a cut-off frequency of 45 Hz and the 2 high-pass filters with a cut-off frequency of 25 Hz are used to extract the sinusoidal precession signal of ^{131}Xe: $\nu_{1L,low}^{(131)} = 45$ Hz and $\nu_{1L,high}^{(129)} = 25$ Hz. The transfer function of the filters is given by $H_{1L}^{(131)}(\nu) = [1/(1 + i\nu/\nu_{1L,low}^{(131)})]^8$ $[(i\nu/\nu_{1L,high}^{(131)})/(1 + i\nu/\nu_{1L_{high}}^{(131)})]^2$. In the second stage lock-in-amplifiers for ^{129}Xe and ^{131}Xe, the low pass filters which have the same cut-off frequency are applied to extract a DC signal which is a function of amplitude and phase of the sinusoidal precession signal. Their frequency responses can be described by the transfer function $H_{2L}(\nu) = [1/(1 + i\nu/\nu_{2L})]^3$ where ν_{2L} is the cut-off frequency of the low pass filter, 1 Hz in our case. The final values after passing through the second stage lock-in-amplifiers are recorded by a computer at a repetition rate of 2 Hz. We note that the FPGA, the references, and the computer operate asynchronously.

4. Data analysis

The NMR frequency shift can be described by using equation (4). We approximate the first stage lock-in-amplifier signal associated with M_x by neglecting fast oscillating terms:

$$y_{1L,x}(t) \approx \int_{-\infty}^{\infty} d\nu H_{1L}(\nu) e^{i\nu t} \int_{-\infty}^{\infty} dt' V_{1L} A(t') e^{-i\nu t'}, \quad (6)$$

where $A(t) = A_0 + A_+ e^{i\omega_{xd}t} + A_- e^{-i\omega_{xd}t} + \delta A(t)$. The coefficients A_0, A_+, and A_- are given as

$$\begin{aligned} A_0 &= \frac{\tau\gamma_{\mathrm{Rb}} M_z^{\mathrm{Rb}}}{4\pi}[-(W\phi_{\mathrm{mod}} + U\theta)B_{\mathrm{res},x} + UB_{\mathrm{res},y}] \\ A_+ &= \frac{\tau\gamma_{\mathrm{Rb}} M_z^{\mathrm{Rb}}}{8\pi}[-(W\phi_{\mathrm{mod}} + U\theta)B_{xd} \\ &\quad + (i(W\phi_{\mathrm{mod}} + U\theta) + U)\psi B_{\mathrm{xe}} e^{i\phi_{\mathrm{xe}}}] \\ A_- &= \frac{\tau\gamma_{\mathrm{Rb}} M_z^{\mathrm{Rb}}}{8\pi}[-(W\phi_{\mathrm{mod}} + U\theta)B_{xd} \\ &\quad + (-i(W\phi_{\mathrm{mod}} + U\theta) + U)\psi B_{\mathrm{xe}} e^{-i\phi_{\mathrm{xe}}}], \end{aligned} \quad (7)$$

where $U = J_1(\xi)(J_2(\xi) + J_0(\xi))$, $W = J_1(\xi)(J_2(\xi) - J_0(\xi))$, and $\theta = (\omega_z^{\mathrm{Rb}} - \omega_{\mathrm{mod}})\tau$. Because $\theta \to 0$ and $\phi_{\mathrm{mod}} \to 0$ are satisfied, we can take the terms up to the first order θ and ϕ_{mod}. Here $\delta A(t)$ describes the white noise, so that its ensemble averaging is 0, $\langle \delta A(t) \rangle = 0$. The useful relation, $\langle \delta A(t+\tau)\delta A(t) \rangle = \sigma_A^2 \delta(\tau)$, helps calculate the power spectral density of $y_{2L,x}(t)$. The averaged signal after the second stage lock-in-amplifier can be written as

$$\begin{aligned} \langle y_{2L,x}(t) \rangle &= \pi |H_{1L}(\omega_{xd})| V_{2L} V_{1L} \\ &\quad \times (A_+ e^{-i(\phi_{xd}+\phi_{1L})} + A_- e^{i(\phi_{xd}+\phi_{1L})}), \end{aligned} \quad (8)$$

where the bracket $\langle ... \rangle$ denotes the ensemble averaging and ϕ_{1L} is the phase of the transfer function $H_{1L}(\nu)$, i.e. $H_{1L}(\nu) = |H_{1L}(\nu)| e^{-i\phi_{1L}}$. For the dispersive mode where the linear response on the frequency change $\Delta\omega$ appears, we carefully choose the demodulation phase ϕ_{xd} to fulfill $\phi_{1L} + \phi_{xd} = \frac{\pi}{2} + \phi'$ and $\phi' \ll 1$. The measured signals as a function of drive frequencies are shown in figures 1(b) and (c). This dispersion curve is essential for measuring the NMR frequency shift.

The NMR frequency shift can be estimated in the on-resonance operation. In the on-resonance case that $\Delta\omega \ll 1/T_2$, we obtain the equations: $\psi = \psi_r \approx \frac{\gamma_{\mathrm{xe}} B_{xd} T_2}{1 + (\gamma_{\mathrm{xe}} B_{xd})^2 T_1 T_2}$ and $\phi_{\mathrm{xe}} \approx \Delta\omega\, T_2$. The signal after the second stage lock-in- amplifier can be written as

$$\begin{aligned} \langle y_{2L,x}(t) \rangle &\approx \frac{\tau\gamma_{\mathrm{Rb}} M_z^{\mathrm{Rb}}}{4} |H_{1L}(\omega_L^{(\mathrm{xe})})| V_{1L} V_{2L} \psi_r B_{\mathrm{xe}} \\ &\quad \times [U(-\phi' + \Delta\omega T_2) + (W\phi_{\mathrm{mod}} + U\theta)]. \end{aligned} \quad (9)$$

Here, we neglect the terms up to the first order. $\omega_L^{(\mathrm{xe})}$ denotes the Larmor frequency of the noble gas atoms. The frequency to signal conversion slope derived from the dispersion curve converts the measured voltage signal to the corresponding NMR frequency, given as

$$\begin{aligned} \eta &= \frac{d\langle y_{2L,x} \rangle}{d\Delta\omega}\Big|_{\Delta\omega=0} \\ &= \frac{\tau\gamma_{\mathrm{Rb}} M_z^{\mathrm{Rb}}}{4} |H_{1L}(\omega_L^{(\mathrm{xe})})| V_{1L} V_{2L} U \psi_r B_{\mathrm{xe}} T_2. \end{aligned} \quad (10)$$

In our experiment, a change of η below 2% was observed during a day under a ± 1 °C room temperature fluctuation. We can easily obtain the frequency shift after dividing the measured $\langle y_{2L,x} \rangle$ signal by the frequency to signal conversion slope:

$$\langle \nu(t) \rangle = \Delta\omega + \frac{-\phi' + \theta + \frac{W}{U}\phi_{\mathrm{mod}}}{T_2}. \quad (11)$$

The second term in equation (11) shows the existence of the frequency offset, due to the phase of the reference signal used in lock-in-amplifiers. The long T_2 time reduces such a frequency offset.

In order to calculate the Allan deviation of the measured NMR frequency shift, we recorded the measured NMR frequency shifts of two Xe isotopes at a repetition rate of 2 Hz. The Allan variance of the second stage lock-in-signal, $y_{2L,x}(t)$, can be written by using its transfer function [23, 24]

$$\sigma_{y_{2L,x}}^2(\tau) = 2\int_0^{\infty} df \frac{\sin^4(\pi f\tau)}{(\pi f\tau)^2} S_{y_{2L,x}}(2\pi f), \quad (12)$$

where $S_{y_{2L,x}}(2\pi f)$ is the power spectral density of $y_{2L,x}(t)$ and can be described by

$$S_{y_{2L,x}}(\nu) = \frac{1}{\sqrt{2\pi}} \int_{-\infty}^{\infty} d\tau \langle y_{2L,x}(t+\tau) y_{2L,x}(t) \rangle e^{-i\nu\tau}, \quad (13)$$

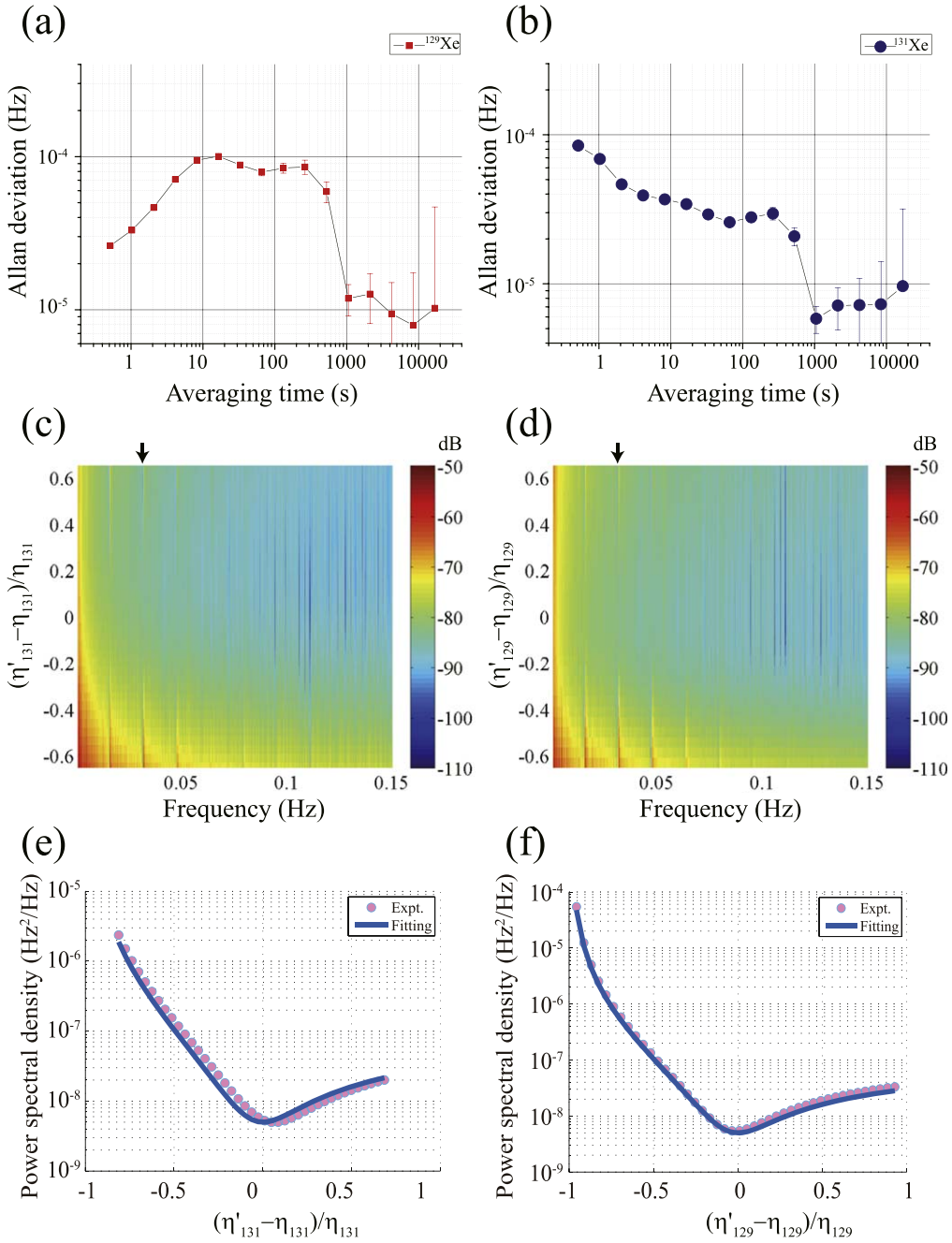

Figure 2. (a) Allan deviation of the ^{129}Xe signal. (b) Allan deviation of the ^{131}Xe signal. (c) Power spectral density in dB scale as a function of frequency and the frequency to signal conversion slope of the ^{131}Xe atoms. The frequency to signal conversion slope of the ^{129}Xe atoms is fixed at η_{129}. (d) Power spectral density in dB scale as a function of frequency and the frequency to signal conversion slope of the ^{129}Xe atoms. The frequency to signal conversion slope of the ^{131}Xe atoms is fixed at η_{131}. (e) Power spectral density as a function of $(\eta'_{131}-\eta_{131})/\eta_{131}$ at 30 mHz indicated by the black arrow in (c). (f) Power spectral density as a function of $(\eta'_{129}-\eta_{129})/\eta_{129}$ at 30 mHz indicated by the black arrow in (d).

where we assume that $\langle y_{2L,x}(t+\tau)y_{2L,x}(t)\rangle$ only depends on the time difference, τ. The bracket $\langle ...\rangle$ represents an ensemble averaging. The Allan deviation of the ^{129}Xe and ^{131}Xe signals mainly depends on the bias magnetic field noise in the on-resonance condition. For convenience of calculation, we decompose $A(t)$ as $A(t) = A_0 + [A_{+,0} + A_{+,d}B_0(t)]e^{i\omega_{xd}t} + [A_{-,0} + A_{-,d}B_0(t)]e^{-i\omega_{xd}t} + \delta A(t)$ where the autocorrelation of the bias magnetic field, $\langle B_0(t+\tau)B_0(t)\rangle$, depends on the time difference, τ. Under the assumption that the cut-off frequency of $H_{2L}(\nu)$ is much smaller than ω_{xd}, i.e. $f_{2L} \ll \omega_{xd}/(2\pi)$, the power spectral density of $y_{2L,x}(t)$ is given as

$$\begin{aligned} S_{y_{2L,x}}(\nu) &\approx \pi^2 V_{1L}^2 V_{2L}^2 |H_{1L}(\omega_{xd})|^2 |H_{2L}(\nu)|^2 \left[\sqrt{\frac{2}{\pi}}\sigma_A^2 \right. \\ &\quad \left. + (-A_{+,d}^2 + 2A_{+,d}A_{-,d} - A_{-,d}^2) S_B(\nu)\right] \\ &= V_{1L}^2 V_{2L}^2 |H_{2L}(\nu)|^2 \left[\sqrt{2\pi^3}|H_{1L}(\omega_{xd})|^2\sigma_A^2 \right. \\ &\quad \left. + \frac{|H_{1L}(\omega_{xd})|^2}{|H_{1L}(\omega_L^{(\mathrm{xe})})|^2}\eta^2\gamma_{\mathrm{xe}}^2 S_B(\nu)\right], \end{aligned} \tag{14}$$

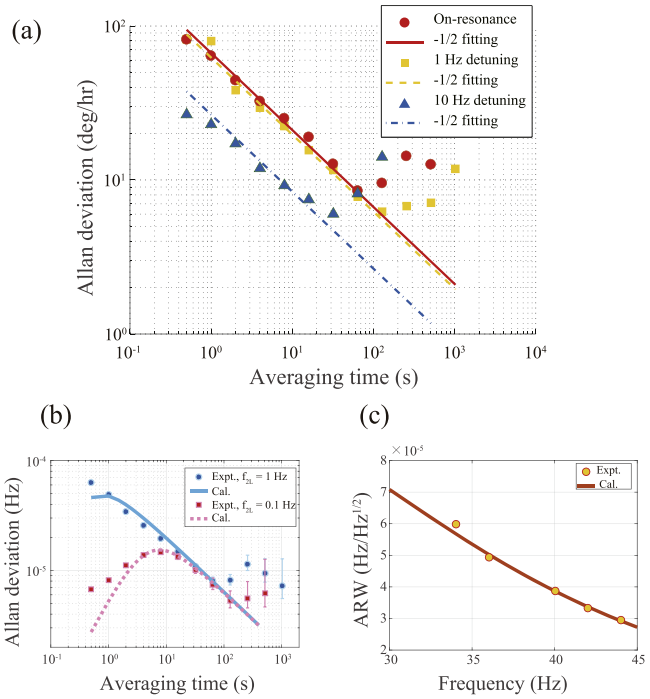

Figure 3. (a) Allan deviation of the rotation rates in the on-resonance case (red circles), in the 1 Hz detuned case (yellow squares), and in the 10 Hz detuned case (blue triangles). The lines depict the Allan deviation of the white noise. (b) Allan deviation of the rotation rate in the two cases: $f_{2L} = 1$ Hz (blue circles) and $f_{2L} = 0.1$ Hz (pink squares). The corresponding calculated Allan deviations are depicted by the lines. (c) Angular random walk as a function of the drive frequencies of ^{131}Xe, $\omega_{xd}^{(131)}$. The red solid line indicates the calculation considering the filter effects, $H_{1L}(\nu)$.

where $S_B(\nu)$ is the power spectral density of the bias magnetic field. We omit the delta function which does not contribute to the Allan deviation. Figures 2(a) and (b) shows the measured Allan deviation of the measured NMR frequency shift of the ^{129}Xe and ^{131}Xe. The white noise characteristic is not shown in the ^{129}Xe atom case (figure 2(a)) due to the magnetic field noise, while only the weak symptom of the white noise arises in the ^{131}Xe atom case, since the ^{129}Xe atoms are more sensitive to the magnetic field than the ^{131}Xe atoms [25].

To distinguish the magnetic field and the rotation rate, the NMR frequency shifts of dual species are combined [5]. The estimator of the rotation rate can be written as

$$\Omega(t) = \frac{\gamma_{131} y_{2L,x}^{(129)}(t)/\eta'_{129} + \gamma_{129} y_{2L,x}^{(131)}(t)/\eta'_{131}}{\gamma_{129} - \gamma_{131}}, \qquad (15)$$

where the superscripts and the subscripts 129 and 131 indicate ^{129}Xe and ^{131}Xe isotopes. η'_{129} and η'_{131} are the given frequency to signal conversion slopes for ^{129}Xe and for ^{131}Xe, respectively. In order to extract the rotation rate precisely the used frequency to signal conversion slope for calculation, η'_{129} (or η'_{131}), has to be same as the real frequency to signal conversion slope, η_{129} (or η_{131}). After some calculation, the power spectral density of $\Omega(t)$ is written as

$$\begin{aligned} S_\Omega(\nu) \approx & \left(\frac{\gamma_{131}\gamma_{129}}{\gamma_{129}-\gamma_{131}}\right)^2 |H_{2L}(\nu)|^2 [S_B(\nu) \\ & \times \left(\frac{\eta_{129}}{\eta'_{129}}\frac{|H_{1L}^{(129)}(\omega_{xd}^{(129)})|}{|H_{1L}^{(129)}(\omega_L^{(129)})|} - \frac{\eta_{131}}{\eta'_{131}}\frac{|H_{1L}^{(131)}(\omega_{xd}^{(131)})|}{|H_{1L}^{(131)}(\omega_L^{(131)})|}\right)^2 \\ & + \sqrt{2\pi^3} V_{1L}^2 V_{2L}^2 |H_{1L}^{(129)}(\omega_{xd}^{(129)})|^2 \left(\frac{\sigma_A^{(129)}}{\eta'_{129}\gamma_{129}}\right)^2 \\ & + \sqrt{2\pi^3} V_{1L}^2 V_{2L}^2 |H_{1L}^{(131)}(\omega_{xd}^{(131)})|^2 \left(\frac{\sigma_A^{(131)}}{\eta'_{131}\gamma_{131}}\right)^2], \end{aligned} \qquad (16)$$

where $\omega_L^{(129)}$ and $\omega_L^{(131)}$ are the Larmor frequencies of ^{129}Xe and of ^{131}Xe, respectively. For the on-resonance operation, the drive frequencies $\omega_{xd}^{(129)}$ and $\omega_{xd}^{(131)}$ are fixed at $\omega_L^{(129)}$ and $\omega_L^{(131)}$, respectively. Equation (15) separates the rotation rate from the measured NMR frequency shift. Figures 2(c) and (d) shows the power spectral density in dB scale as a function of the frequency to signal conversion slopes and frequencies. The power spectral density $S_\Omega(\nu)$ can be calculated by fast Fourier transform of the autocorrelation of $\Omega(t)$. Several peaks, originating from the long-term magnetic noise, arise in the two-dimensional graph. For example, around a frequency of 30 mHz, indicated by the black arrows in figures 2(c) and (d), the power spectral density as a function of $(\eta'_{131} - \eta_{131})/\eta_{131}$ (or $(\eta'_{129} - \eta_{129})/\eta_{129}$) is shown in figure 2(e) (or in figure 2(f)). From equation (16), we can derive the fitting formula, $y = p_0(\eta_{129}/\eta'_{129} - \eta_{131}/\eta'_{131})^2 + y_0$ where p_0 and y_0 are constants. The experimental results are well fitted with the derived formula. The noise spectrum is maximally reduced when $\eta'_{129} = \eta_{129}$ and $\eta'_{131} = \eta_{131}$. At this condition, the term including $S_B(\nu)$ becomes zero so that the Allan variance can be written as

$$\begin{aligned} \sigma_\Omega^2(\tau) \approx & \sqrt{8\pi^3}\left(\frac{\gamma_{131}\gamma_{129}}{\gamma_{129}-\gamma_{131}}\right)^2 \left(\frac{4}{\tau\gamma_{\mathrm{Rb}} M_z^{\mathrm{Rb}} U}\right)^2 \\ & \times \left[\left(\frac{\sigma_A^{(129)}}{B_{\mathrm{xe}}^{(129)} T_2^{(129)} \psi_r^{(129)} \gamma_{129}}\right)^2 + \left(\frac{\sigma_A^{(131)}}{B_{\mathrm{xe}}^{(131)} T_2^{(131)} \psi_r^{(131)} \gamma_{131}}\right)^2\right] \\ & \times \int_0^\infty df \frac{\sin^4(\pi f\tau)}{(\pi f\tau)^2} |H_{2L}(2\pi f)|^2. \end{aligned} \qquad (17)$$

Only the white noise terms survive. In the off-resonance operation, the Allan variance is governed by the white noise term because $A_{+,d}$ and $A_{-,d}$ are zero. Particularly, in the slightly off-resonance operation that $|H_{1L}^{(129)}(\omega_{xd}^{(129)})| \approx |H_{1L}^{(129)}(\omega_L^{(129)})|$ and $|H_{1L}^{(131)}(\omega_{xd}^{(131)})| \approx |H_{1L}^{(131)}(\omega_L^{(131)})|$, the Allan variance can be also described by equation (17). Figure 3(a) shows the Allan deviations of the measured rotation rate in the on- and the 1 Hz off-resonance case (slightly off-resonance). The Allan deviation of the on-resonance case is well overlapped with that of the off-resonance case, implying that the subtraction of the magnetic field noise is well operated.

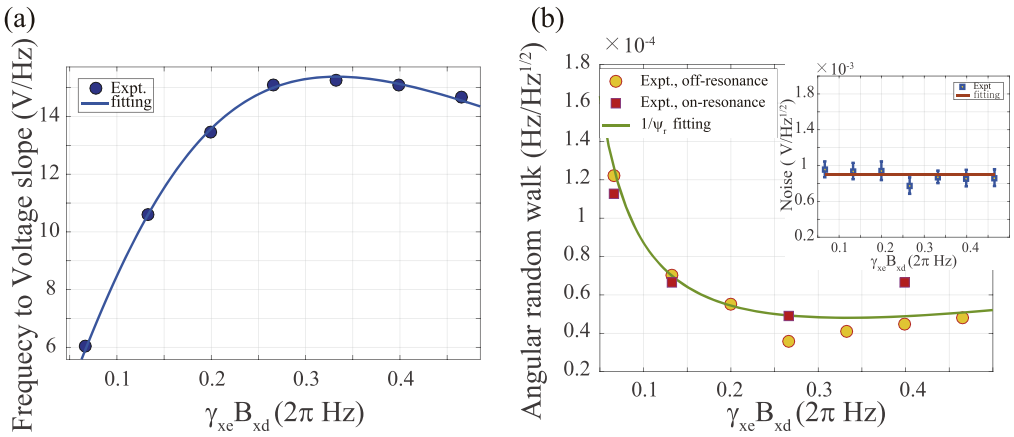

Figure 4. (a) Frequency to signal conversion slope as a function of B_{xd}. The solid line depicts the fitting of $\psi_r = x/(1 + px^2)$. (b) Angular random walk as a function of B_{xd} in the 1 Hz detuned case (yellow circles) and in the on-resonance case (red squares). The green solid line results from the $1/\psi_r = (1 + px^2)/x$ fitting. The inset shows the noise as a function of B_{xd}. The noise remains constant.

Table 1. 1 Hz off-resonance signal noises and the corresponding angular random walks.

Species	Noise(mV Hz$^{-1/2}$)	Slope(V Hz^{-1})	ARW(deg h$^{-1/2}$)
^{129}Xe	1.3	782.5	0.036
^{131}Xe	0.923	−14.32	1.39

5. Discussions

The NMR frequency shift measurement is affected by the filters in lock-in-amplifiers [14]. In our calculation, the effect of the low pass filter in the second stage lock-in-amplifier, described by $|H_{2L}(\nu)|$, is included in equation (17). In figure 3(b) we compare the two cases of the different cut-off frequencies, $f_{2L} = 1$ Hz and $f_{2L} = 0.1$ Hz. The calculations considering only the white noise term are well overlapped with the experimental data. In particular, a peak arises at an averaging time of $1/f_{2L}$ because the low pass filter of the second stage lock-in-amplifier reduces the noise of frequencies above f_{2L}.

We also investigated the effect of the filters in the first stage lock-in-amplifier by changing the detuning of the transverse AC drive field. Figure 3(a) shows a comparison between the Allan deviations of the 1 Hz detuning and of the 10 Hz detuning. The angular random walk of the 10 Hz detuning case is 2 times smaller than that of the 1 Hz detuning due to the effect of the filters in the first stage lock-in-amplifier. The angular random walk of the rotation rate is mainly determined by that of the NMR frequency for the small gyromagnetic ratio species [14]. Moreover, the ratio of the frequency to signal conversion slopes is given as $\eta'_{129}/\eta'_{131} = 54.6$ in our experiment so that it is enough to consider only the $\sigma_A^{(131)}$ term in equation (16), the white noise of the ^{131}Xe signal. As a result, the angular random walk of the rotation rate is proportional to $|H_{1L}^{(131)}(\omega_{xd}^{(131)})|$. We obtain the amplitude ratio of the transfer function, $|H_{1L}^{(131)}(\omega_L^{(131)} + 2\pi \times 1\ Hz)|/|H_{1L}^{(131)}(\omega_L^{(131)} + 2\pi \times 10$ Hz)$| = 1.99$. It is consistent with the angular random walk ratio of the two detuning cases, given as 2. More generally, figure 3(c) shows the angular random walk of the NMR frequency shift of ^{131}Xe as a function of the drive frequencies. The experimental data is well fitted by $|H_{1L}^{(131)}(\omega)|$. The careful selection of the drive frequency, or a post correction considering the transfer function of the band pass filter, is therefore required to reveal the magnetic field noise-free limit of the angular random walk for the rotation rate. We used a 1 Hz detuning to verify the angular random walk limit in our experiment. Although 1 Hz detuning seems insufficient, the long transverse relaxation time T_2 of several tens of second makes the system insensitive to the magnetic field noise because $\frac{\Delta\omega T_2}{2\pi} \gg 1$.

In our experiment, the white noise mainly contributes to the angular random walk for the rotation rate. To decrease the angular random walk in this regime, a large frequency to signal conversion slope is required. The frequency to signal conversion slope is determined by various parameters such as T_2, B_{xe}, ψ_r, and U. Among them, we optimized ψ_r by changing B_{xd}. Figure 4(a) shows the frequency to signal conversion slope as a function of B_{xd}. It increases with B_{xd} and decreases after passing the maximum point due to the T_1 decay. The measured frequency to signal conversion slope is well fitted by $\psi_r = x/(1 + px^2)$ where $x = \gamma_{xe}B_{xd}$. Also, the angular random walk is investigated as a function of B_{xd} in figure 4(b). It is well overlapped with the inverse of ψ_r, $(1 + px^2)/x$. Such a ψ_r optimization works well in a regime where the noise remains constant against changing B_{xd}. The inset of figure 4(b) shows that the noise is independent of B_{xd}.

Table 1 shows the noises and the corresponding angular random walks after the ψ_r optimization in the slightly off-resonance operation. It shows that the angular random walk of our gyroscope is limited by the noise of the ^{131}Xe signal. The rotation extraction gives the composite angular random walk, 1.072 deg h$^{-1/2}$ which is very close to the on-resonance angular random walk, 1.113 deg h$^{-1/2}$. Despite having a lower noise than the ^{129}Xe signal, the slow frequency-signal conversion slope for ^{131}Xe leads the noise of 64.45 μHz$^{1/2}$. The

converted angular random walk is 1.39 deg $h^{-1/2}$. The slow slope of the ^{131}Xe signal is caused by the short T_2 time and the small magnetic field from the ^{131}Xe atoms, already reported in [26]. To overcome the current angular random walk, an atomic cell filled with high pressure ^{131}Xe gas is required to increase B_{xe} from the ^{131}Xe atoms. Additionally, identifying the origins of the white noise and decreasing their contribution to σ_A will help to reach a low angular random walk. Ultimately, an angular random walk is limited by atomic projection noise and laser shot noise [27].

6. Conclusion

We analyzed the NMR frequency shift measurements realized by two stage lock-in-amplifiers. The Allan deviations of the NMR frequency shifts and of the rotation rate were investigated during on- and off-resonance operation, theoretically and experimentally. The filter effects of the lock-in-amplifier were revealed in our analysis. The angular random walk of our experimental setup, 1.11 deg $h^{-1/2}$, was mainly limited by the white noise of the ^{131}Xe signal which was verified by the slightly off-resonance operation.

Acknowledgments

This work was supported by a grant to Atom Optic Sensor Laboratory for National Defense funded by Defense Acquisition Program Administration and Agency for Defense Development.

Appendix

Table A1. Summary of symbols related to ^{87}Rb.

Symbols	Description	Typical value	Notes
γ_{Rb}	Gyromagnetic ratio of ^{87}Rb	$2\pi \times 6998\ \mathrm{Hz}/\mu\mathrm{T}$	
τ	Lifetime of ^{87}Rb spins	Order of 10 ms	
B_0	DC bias B-field	9.95 μT	
B_{mod}	Amplitude of the AC bias B-field	10 μT	
M_z^{Rb}	Magnetic moment of ^{87}Rb	—	
ω_z^{Rb}	Larmor frequency of ^{87}Rb	$2\pi \times 69.63$ kHz	$\omega_z^{Rb} = \gamma_{Rb} B_0$
ω_{amp}	Amplitude of the bias B-field modulation	$2\pi \times 70$ kHz	$\omega_{amp} = \gamma_{Rb} B_{mod}$
ω_{mod}	Angular frequency of the bias B-field modulation	$2\pi \times 69.63$ kHz	$\omega_{mod} = \omega_z^{Rb}$, B_y sensing mode
ϕ_{mod}	Phase of the bias B-field modulation	$\approx$0 rad	B_y sensing mode
ξ	Ratio of the amplitude of the bias B-field modulation to the modulation frequency	$\approx$1	$\xi = \omega_{amp}/\ \omega_{mod}$

Table A2. Summary of symbols related to Xe. The indices 129 and 131 indicate the Xe isotopes, ^{129}Xe and ^{131}Xe.

Symbols	Description	Symbols for Xe isotopes and typical value	Notes
γ_{xe}	Gyromagnetic ratio of Xe	$\gamma_{129} = 2\pi \times 11.86\ \mathrm{Hz}/\mu\mathrm{T}$ $\gamma_{131} = 2\pi \times 3.52\ \mathrm{Hz}/\mu\mathrm{T}$	
$\omega_L^{(xe)}$	Larmor frequency of Xe	$\omega_L^{(129)} = 2\pi \times 118.15$ Hz $\omega_L^{(131)} = 2\pi \times 35.0225$ Hz	$\omega_L^{(xe)} = \gamma_{xe} B_0$
ω_{xd}	Angular frequency of the transverse AC B_x field	$\omega_{xd}^{(129)} = 2\pi \times 118.15$ Hz $\omega_{xd}^{(131)} = 2\pi \times 35.0225$ Hz	$\omega_{xd} = \omega_L^{(xe)}$ resonance condition
B_{xd}	Amplitude of the transverse AC B_x field	$B_{xd}^{(129)} = 0.5$ nT $B_{xd}^{(129)} = 10$ nT	
ϕ_{xd}	Phase delay of the transverse AC B_x field	$\phi_{xd}^{(129)} \approx 280°$ $\phi_{xd}^{(131)} \approx 320°$	$\phi_{1L} + \phi_{xd} = \pi/2$ dispersion mode
ϕ_{xe}	Phase delay of the Xe induced magnetic field	$\phi_{xe}^{(129)}$ $\phi_{xe}^{(131)}$	$\tan(\phi_{xe}) = \Delta\omega T_2$
η	Frequency to signal conversion slope	η_{129} η_{131}	

Table A2. (Continued.)

Symbols	Description	Symbols for Xe isotopes and typical value	Notes
η'	Given frequency to signal	$\eta'_{129} \approx \eta_{129}$	Precise rotation
P	conversion slope	$\eta'_{131} \approx \eta_{131}$	extraction condition
σ_A	Power spectral density	$\sigma_A^{(129)}$	
	of white noise	$\sigma_A^{(131)}$	
B_{xe}	Nuclear magnetic field	$B_{\mathrm{xe}}^{(129)} = 100$ nT	
	from Xe	$B_{\mathrm{xe}}^{(131)} = 9$ nT	
T_1	Longitudinal spin	$T_1^{(129)} = 27$ s	~100 °C
	relaxation time	$T_1^{(131)} = 12$ s	
T_2	Transverse spin	$T_2^{(129)} = 20$ s	~100 °C
	relaxation time	$T_2^{(131)} = 9$ s	
ψ_r	Tip angle	$\psi_r^{(129)}$	$\psi_r = \frac{\gamma_{\mathrm{xe}} B_{xd} T_2}{1 + (\gamma_{\mathrm{xe}} B_{xd})^2 T_1 T_2}$
	of the Xe nuclear magnetic moment	$\psi_r^{(131)}$	
$H_{1L}(\nu)$	Transfer function	$H_{1L}^{(129)}(\nu)$	
	of the first lock-in-amplifier	$H_{1L}^{(131)}(\nu)$	
$H_{2L}(\nu)$	Transfer function	$H_{2L}^{(129)}(\nu)$	$H_{2L}^{(129)}(\nu) = H_{2L}^{(131)}(\nu)$
	of the first lock-in-amplifier	$H_{2L}^{(131)}(\nu)$	$= H_{2L}(\nu)$

ORCID iDs

Sangkyung Lee https://orcid.org/0000-0002-8094-3230

References

[1] Walker T G and Happer W 1997 *Rev. Mod. Phys.* **69** 629
[2] Nikolaou P *et al* 2013 *Proc. Natl Acad. Sci.* **110** 14150
[3] Jiménez-Martínez R, Kenney D J, Rosenbluh M, Donley E A, Knappe S, Seltzer S J, Ring H L, Bajaj V S and Kitching J 2014 *Nat. Commun.* **5** 3908
[4] Kominis I K, Kornack T W, Allred J C and Romalis M V 2003 *Nature* **422** 596
[5] Grover B C, Kanegsberg E, Mark J G and Meyer R L 1979 *US Patent* 4157495
[6] Kornack T W, Ghosh R K and Romalis M V 2005 *Phys. Rev. Lett.* **95** 230801
[7] Meyer D and Larsen M 2014 *Gyroscopy Navig.* **5** 75
[8] Fang J and Qin J 2012 *Sensors* **12** 6331
[9] Smiciklas M, Brown J M, Cheuk L W, Smullin S J and Romalis M V 2011 *Phys. Rev. Lett.* **107** 171604
[10] Bulatowicz M, Griffith R, Larsen M, Mirijanian J, Fu C B, Smith E, Snow W M, Yan H and Walker T G 2013 *Phys. Rev. Lett.* **111** 102001
[11] Noor R M and Shkel A M 2018 *J. Microelectromech. Syst.* **27** 1148
[12] Fang J, Wan S, Qin J, Zhang C, Quan W, Yuan H and Dong H 2013 *Rev. Sci. Instrum.* **84** 083108
[13] Allred J C, Lyman R N, Kornack T W and Romalis M V 2002 *Phys. Rev. Lett.* **89** 130801
[14] Walker T G and Larsen M S 2016 *Adv. At. Mol. Opt. Phys.* **65** 373
[15] Donley E A 2010 *SENSORS, 2010 IEEE (Kona, HI)* 17-22
[16] Appelt S, Ben-Amar Baranga A, Erickson C J, Romalis M V, Young A R and Happer W 1998 *Phys. Rev.* A **58** 1412
[17] Li Z, Wakai R T and Walker T G 2006 *Appl. Phys. Lett.* **89** 134105
[18] Jiang L, Quan W, Li R, Fan W, Liu F, Qin J, Wan S and Fang J 2018 *Appl. Phys. Lett.* **112** 054103
[19] Grover B C 1978 *Phys. Rev. Lett.* **40** 391
[20] Kwon T M and Debley W P 1984 *US Patent* 4450407
[21] Yim S H, Kim Z, Lee S, Kim T H and Shim K H 2018 *Rev. Sci. Instrum.* **89** 116102
[22] Carr H Y and Purcell E M 1954 *Phys. Rev.* **94** 630
[23] Rutman J 1974 *IEEE Trans. Instrum. Meas.* **23** 40
[24] Witt T J 2001 *IEEE Trans. Instrum. Meas.* **50** 445
[25] Liu X, Chen C, Qu T, Yang K and Luo H 2016 *Sci. Rep.* **6** 24122
[26] Donley E A, Long J L, Liebisch T C, Hodby E R, Fiser T A and Kitching J 2009 *Phys. Rev.* A **79** 013420
[27] Vershovskii A K, Litmanovich Y A, Pazgalev A S and Pesheknonov V G 2018 *Gyroscopy Navig.* **9** 162